Nonequilibrium-relaxation approach to quantum phase transitions: Nontrivial critical relaxation in cluster-update quantum Monte Carlo

Yoshihiko Nonomura[*]

International Center for Materials Nanoarchitectonics, National Institute for Materials Science, Tsukuba, Ibaraki 305-0044, Japan

Yusuke Tomita[†]

College of Engineering, Shibaura Institute of Technology, Saitama 337-8570, Japan

Although the nonequilibrium-relaxation (NER) method has been widely used in Monte Carlo studies on phase transitions in classical spin systems, such studies have been quite limited in quantum phase transitions. The reason is that the relaxation process based on cluster-update quantum Monte Carlo (QMC) algorithms, which are now standards in Monte Carlo studies on quantum systems, has been considered "too fast" for such analyses. Recently, the present authors revealed that the NER process in classical spin systems based on cluster-update algorithms is characterized by stretched-exponential critical relaxation, rather than conventional power-law relaxation in local-update algorithms. In the present article, we show that this is also the case in quantum phase transitions analyzed with the cluster-update QMC. As the simplest example of isotropic quantum spin models that exhibit quantum phase transitions, we investigate the Néel-dimer quantum phase transition in the two-dimensional $S = 1/2$ columnar-dimerized antiferromagnetic Heisenberg model with the continuous-time loop algorithm, and we confirm stretched-exponential critical relaxation consistent with the three-dimensional classical Heisenberg model in the Swendsen-Wang algorithm.

I. INTRODUCTION

Monte Carlo (MC) simulations have been widely utilized in statistical-mechanical studies on classical spin systems, where the Boltzmann weight for a MC flip is determined locally. In quantum spin systems, the Boltzmann weight cannot be determined locally unless diagonalizing the Hamiltonian matrix in principle, and treatable system sizes are strictly reduced. This difficulty was overcome by introducing the Suzuki-Trotter decomposition [1,2], where noncommutable exponential operators are approximately divided into n Trotter layers, and the original system is reproduced in the $n \to \infty$ limit. This procedure can be regarded as an introduction of an extra imaginary-time axis.

In the original quantum Monte Carlo (QMC) formulation [2], the $n \to \infty$ limit was taken by numerical extrapolation with several finite-n systems, and nontrivial global-update processes should be introduced additionally by hand in order to maintain ergodicity. Such a complicated procedure was simplified by the continuous-time QMC algorithm [3], where the $n \to \infty$ limit is taken as part of the formulation without numerical extrapolation. This QMC algorithm should be coupled with cluster-update QMC algorithms such as the loop algorithm [4], the worm algorithm [5], or the

directed-loop algorithm [6], in which ergodicity is ensured within the formulation.

The nonequilibrium-relaxation (NER) method [7] is one of the MC approaches to investigate phase transitions. In contrast to other approaches such as the cluster algorithms [8,9] and extended ensemble methods [10–12], the critical slowing down is not avoided but rather utilized in this scheme for the evaluation of critical phenomena. The critical point is estimated from the power-law behavior of physical quantities expected there, and the critical exponents are evaluated from the exponents of such relaxation behaviors. This relaxation process is usually terminated much earlier than arrival at equilibrium. To avoid artifacts originating from biased initial states, completely ordered or completely disordered states are usually chosen as initial states.

In equilibrium MC simulations, thermal averaging is taken during long-time measurement after discarding equilibration data. In NER calculations, such averaging is replaced by that for independent random-number sequences (RNSs), i.e., many MC runs based on different initial seeds of pseudorandom numbers are averaged [13], and all the numerical data are utilized.

Several attempts to generalize the NER scheme to the above-mentioned modern QMC algorithms have not been successful so far, and cluster-update QMC algorithms have been considered "too fast" for NER. Successful examples of the application of NER to QMC were based on a world-line local-update QMC algorithm with finite Trotter layers [14] or a continuous-time QMC algorithm only along the

———————
[*]nonomura.yoshihiko@nims.go.jp
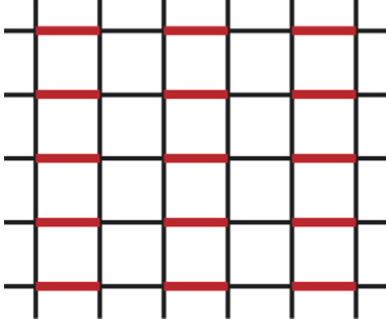[†]ytomita@shibaura-it.ac.jp

FIG. 1. Schematic figure of the columnar dimer pattern. Broad red lines represent the dimerized bonds.

imaginary-time axis [15], both of which simply slowed down relaxation to fit for power-law NER. The advantage of NER is canceled by these redundant procedures, because numerical costs of equilibrium calculations in modern QMC are comparable to those of NER calculations based on the slowed-down algorithms.

Recently, the present authors numerically found that the early-time nonequilibrium critical relaxation in cluster algorithms is described by the stretched-exponential simulation-time dependence, not by the power-law one in various classical spin systems [16–18]. The NER framework for cluster algorithms can be constructed on the basis of this relaxation formula. Quite recently, the present authors derived this relaxation formula phenomenologically in the Ising models in the Swendsen-Wang algorithm [19].

In the present article, we introduce an NER analysis of quantum phase transitions based on the continuous-time loop algorithm. Although this algorithm is based on a cluster update, it is not trivial whether the stretched-exponential critical relaxation occurs in the present one-dimensional loop clusters, which is different from bulky ones in cluster algorithms in classical spin systems.

The outline of the rest of the present article is as follows. In Sec. II, the model and procedures of numerical calculations are summarized. Numerical results are reported in Sec. III, which is divided into two subsections with respect to physical quantities, namely the absolute value of the Néel order and staggered susceptibility. The above descriptions are summarized in Sec. IV, and essential merits of the present scheme are discussed.

II. MODEL AND METHOD

In the present article, we study the two-dimensional $S = 1/2$ columnar-dimerized antiferromagnetic Heisenberg model on a square lattice,

$$\mathcal{H} = \sum_{\langle ij \rangle \in \text{n.n.}} J_{ij} \vec{S}_i \cdot \vec{S}_j, \ S = 1/2, \tag{1}$$

$$J_{ij} = \begin{cases} (1 + \delta)J & \text{on dimerized bonds } (\delta \geqslant 0), \\ J & \text{elsewhere,} \end{cases} \tag{2}$$

with the nearest-neighbor interaction and the columnar dimer pattern shown in Fig. 1. For $\delta = 0$ (the uniform case), this model has the Néel order (reduced due to quantum fluctuations) in the ground state. For large enough δ, singlet pairs

on the dimerized bonds wipe out the Néel order. There exists a critical point δ_c between the two cases, and this quantum phase transition is of conventional second order, because the dimerization does not accompany spontaneous symmetry breaking.

This is the simplest isotropic quantum spin model with quantum phase transition without frustration. This model has been intensively studied with QMC [20–22], and its universality class has been considered to be the same as that of the three-dimensional (3D) classical Heisenberg model. Here we analyze the early-time relaxation behavior of this model with the continuous-time loop algorithm. In the NER analysis, the choice of the initial state is crucial. In the 3D classical Heisenberg model, we found that the ordering process from the perfectly disordered state results in much smaller deviation from the stretched-exponential critical relaxation than the decaying process from the perfectly ordered state [18].

In classical spin systems, the perfectly disordered state is realized for $T \to \infty$. However, when NER calculations are started from classical perfectly disordered states (spin configurations are perfectly random along the spatial directions but perfectly aligned along the imaginary-time direction) in quantum phase transitions in antiferromagnets formulated with the Ising basis (i.e., $S_i^z = \pm 1/2$), spin configurations quickly converge to the classical Néel state first, and then gradually arrive at equilibrium in the vicinity of the Néel-ordered region. The physical background of this relaxation process is as follows: spins aligned along the imaginary-time direction form a loop cluster, while gate insertion only takes place between antiparallel spin configurations. Therefore, classical spin flip to the classical Néel state occurs first and further relaxation by gate insertion follows, because the classical Néel state consists of antiparallel spin configurations.

In the present study, MC time evolution is based on the standard loop algorithm; loop clusters are generated in the whole system, and each cluster is flipped with 50% probability, similarly to the Swendsen-Wang algorithm in classical spin systems [8]. When cluster flips are once attempted over the whole system, it is regarded as a Monte Carlo step (MCS), which is the unit of simulation time. We start from the isolated dimer state, in which only singlet pairs are on the dimerized bonds, and it becomes the ground state in the $\delta \to \infty$ limit. Since the parameter δ plays a role of temperature in this quantum phase transition, this process corresponds to NER from a perfectly disordered state. Note that this quantum state is described by the linear combination of Ising bases, and each QMC simulation starts from one of the typical classical states. The "sample average" of such states is taken during simulations together with the RNS average.

In the present study, we analyze the absolute value of the Néel order and staggered susceptibility,

$$|m_N| \equiv \frac{1}{N} \left| \sum_i (-1)^i S_i^z \right|, \tag{3}$$

$$\chi_{st} \equiv \frac{1}{N} \sum_{i,j} (-1)^{i-j} S_i^z S_j^z, \tag{4}$$

with abbreviations $i \equiv (i_x, i_y)$ and $(-1)^i \equiv (-1)^{i_x + i_y}$, and we do not take the summation along the imaginary-time direction

(i.e., only on the initial Trotter layer). In QMC simulations of antiferromagnets on bipartite lattices, the original Hamiltonian (1) is transformed to

$$\mathcal{H} = \sum_{\langle ij \rangle \in \text{n.n.}} J_{ij}\left(-S_i^x S_j^x - S_i^y S_j^y + S_i^z S_j^z\right), \ S = 1/2, \quad (5)$$

with the spin rotation $S_i^x \rightarrow -S_i^x$, $S_i^y \rightarrow -S_i^y$, $S_i^z \rightarrow S_i^z$ on one of the sublattices to remove the negative sign. Then, the singlet state on each dimerized bond is transformed from $(|\uparrow\downarrow\rangle - |\downarrow\uparrow\rangle)/\sqrt{2}$ to $(|\uparrow\downarrow\rangle + |\downarrow\uparrow\rangle)/\sqrt{2}$ in actual simulations, and states in the Ising basis contributing to the isolated dimer state are sampled as follows:

(i) Consider the system with $J_{ij} = (1 + \delta)J$ on dimerized bonds and $J_{ij} = 0$ elsewhere.

(ii) Assign the state $|\uparrow\downarrow\rangle$ or $|\downarrow\uparrow\rangle$ on each dimerized bond randomly but to keep the Néel order (3) vanishing on the initial Trotter layer, on which physical quantities are measured. (When the RNS average is taken, this initial configuration is also changed.)

(iii) Insert gates along the imaginary-time direction [23] on each dimerized bond with the probability corresponding to $J_{ij} = (1 + \delta)J$. A pair of gates generates a loop cluster, and the loop should be closed when it crosses the periodic boundary along the imaginary-time direction. Then, the number of gates is taken to be even on each dimerized bond.

(iv) Flip the basis $|\uparrow\downarrow\rangle$ to $|\downarrow\uparrow\rangle$ and vice versa at each gate. [When steps (iii) and (iv) are skipped, we have one of the classical perfectly disordered states.]

When the stretched-exponential critical relaxation holds, early-time behaviors of the absolute value of the Néel order and staggered susceptibility at the quantum critical point δ_c are expected to be given by

$$\langle |m_N(t, L)| \rangle \sim L^{-d/2} \exp\left(+c_m t^\sigma\right), \quad (6)$$

$$\langle \chi_{st}(t, L) \rangle \sim \exp\left(+c_\chi t^\sigma\right), \quad (7)$$

with the RNS average $\langle \cdots \rangle$, simulation time t, linear size $L_x = L_y = L$, spatial dimension $d = 2$ (this size dependence originates from the normalized random-walk growth of spin clusters), quantity-dependent coefficients c_m and c_χ, and relaxation exponent σ ($0 < \sigma < 1$) common in all the physical quantities. Combining these formulas with the equilibrium finite-size scaling relations, namely $\langle |m_N(t = \infty, L)| \rangle \sim L^{-\beta/\nu}$ and $\langle \chi_{st}(t = \infty, L) \rangle \sim L^{\gamma/\nu}$, we arrive at the following nonequilibrium-to-equilibrium scaling relations:

$$\langle |m_N(t, L)| \rangle L^{\beta/\nu} \sim f_m(c_m t^\sigma - \ln L^{d/2 - \beta/\nu}), \quad (8)$$

$$\langle \chi_{st}(t, L) \rangle L^{-\gamma/\nu} \sim f_\chi(c_\chi t^\sigma - \ln L^{\gamma/\nu}), \quad (9)$$

with scaling functions f_m and f_χ [16,18].

III. NUMERICAL RESULTS

A. Absolute value of Néel order

First, we analyze the absolute value of the Néel order and evaluate the quantum critical point δ_c, critical exponent β/ν, and relaxation exponent σ. As an example, this quantity multiplied with $L^{d/2}$ at $\delta = 0.909\,47$ (as will be shown below, the most probable value of δ_c) is plotted versus simulation
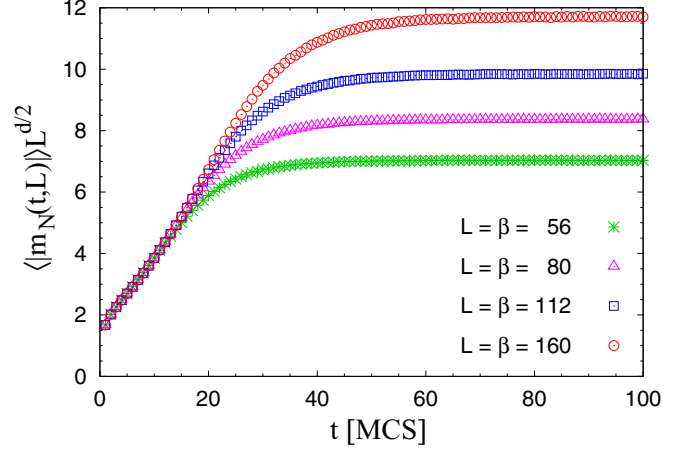

FIG. 2. Simulation-time dependence of the absolute value of the Néel order at $\delta = 0.909\,47$ for $L = \beta = 56$ (green stars), 80 (pink triangles), 112 (blue squares), and 160 (red circles). Error bars are much smaller than symbols in this scale.

time in Fig. 2 for $L = 56$ (2.56×10^6 RNS are averaged), 80 (2.56×10^6 RNS), 112 (1.28×10^6 RNS), and 160 (0.64×10^6 RNS), where the system size along the imaginary-time axis is taken the same as those along the real axes, namely $\beta \equiv 1/(k_B T) = L$. Similarly to the previous cluster NER studies on classical spin systems, we find that this quantity is scaled well with Eq. (6) initially, and tends to be away from this equation and to saturate as t increases.

The data in Fig. 2 are scaled with Eq. (8) in Fig. 3 with $\beta/\nu = 0.514(1)$, $\sigma = 0.502(8)$, and $c_m = 0.423(14)$. The exponent β/ν is evaluated from the scaling behavior in the vicinity of equilibrium, which little depends on the
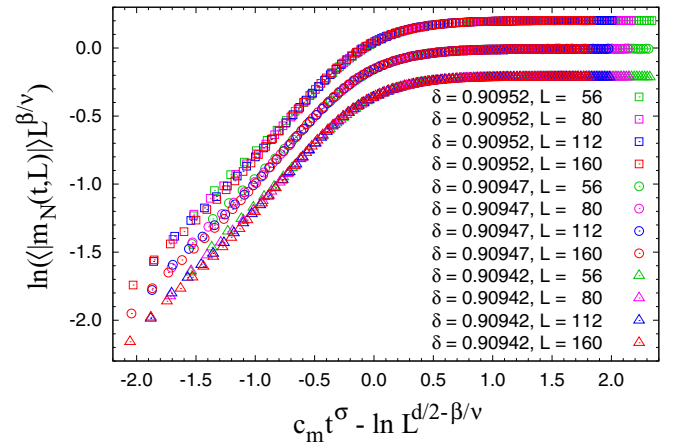

FIG. 3. Nonequilibrium-to-equilibrium scaling plot of the absolute value of the Néel order at $\delta = 0.909\,47$ (circles) for $L = \beta = 56$ (green symbols), 80 (pink symbols), 112 (blue symbols), and 160 (red symbols) with $\beta/\nu = 0.514(1)$, $\sigma = 0.502(8)$, and $c_m = 0.423(14)$. The data at $\delta = 0.909\,52$ (squares) and $0.909\,42$ (triangles) for the same sizes are scaled with $\beta/\nu = 0.516(1)$, $\sigma = 0.501(9)$, $c_m = 0.427(18)$ and $\beta/\nu = 0.512(1)$, $\sigma = 0.504(6)$, $c_m = 0.421(10)$, respectively. Error bars are much smaller than symbols in this scale. The data except for $\delta = 0.909\,47$ are shifted upward or downward for clear visualization.
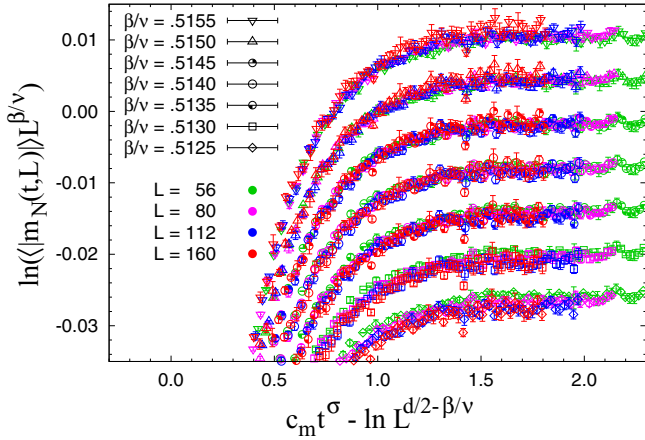
FIG. 4. Nonequilibrium-to-equilibrium scaling plot of the absolute value of the Néel order at $\delta = 0.909\,47$ in the vicinity of equilibrium for $\beta/\nu = 0.5125$ (diamonds), 0.5130 (squares), 0.5135 (downside-marked circles), 0.5140 (circles), 0.5145 (upside-marked circles), 0.5150 (triangles), and 0.5155 (inverse triangles) with the same colors for $L = \beta = 56$, 80, 112, and 160 as those in Fig. 3 using $\sigma = 0.502$ and $c_m = 0.423$ used in Fig. 3 at the same δ. The data except for $\beta/\nu = 0.5140$ are shifted upward or downward for clear visualization.

values of σ and c_m. The procedure to evaluate the error bar of β/ν is visualized in Fig. 4, where the data in the vicinity of equilibrium at $\delta = 0.909\,47$ in Fig. 3 are plotted for $\beta = 0.5125$ (diamonds), 0.5130 (squares), 0.5135 (downside-marked circles), 0.5140 (circles; only these data are shown in Fig. 3), 0.5145 (upside-marked circles), 0.5150 (triangles), and 0.5155 (inverse triangles) with the same colors for $L = 56$, 80, 112, and 160 as those in Fig. 3. The values of σ and c_m are evaluated for each β/ν so as to minimize the mutual residue of the data with Eq. (8), and they are almost unchanged for such a small variance of β/ν. Thus, common σ and c_m are used in this figure. These data are still on the same curve at $\beta/\nu = 0.5135$ and 0.5145, and clearly out of scaling at $\beta/\nu = 0.5125$ and 0.5155. Behaviors at $\beta/\nu = 0.513$ and 0.515 seem on the edge of out-of-scaling, and it would be fair to take the final error bar as $\beta/\nu = 0.514(1)$. In Ref. [18], we also used the criterion that the early-time behavior is described by the stretched-exponential relaxation formula (6), and the slope of the scaled data should be unity in the region $c_m t^\sigma - \ln L^{d/2 - \beta/\nu} \lesssim -0.5$ in Fig. 3. Here we do not use this criterion, because the validity of this formula cannot be fully justified [24].

To evaluate the quantum critical point δ_c, the data in the vicinity of equilibrium for $L = 56$ (green symbols), 80 (pink symbols), 112 (blue symbols), and 160 (red symbols) at $\delta = 0.909\,54$ (diamonds with $\beta/\nu = 0.517$), 0.909 52 (squares with $\beta/\nu = 0.516$), 0.909 47 (circles with $\beta/\nu = 0.514$), 0.909 42 (triangles with $\beta/\nu = 0.512$), and 0.909 40 (inverse triangles with $\beta/\nu = 0.511$) are plotted in Fig. 5 using $\sigma = 0.502$ and $c_m = 0.423$ estimated at $\delta = 0.909\,47$ in Fig. 3. The data at $\delta = 0.909\,52$ and 0.909 42 seem on the edge of scaling with $\beta = 0.516(1)$, $\sigma = 0.501(9)$, $c_m = 0.427(18)$ and $\beta = 0.512(1)$, $\sigma = 0.504(6)$, $c_m = 0.421(10)$, respectively (see Fig. 3), while the data at $\delta = 0.909\,54$ and 0.909 40 are clearly
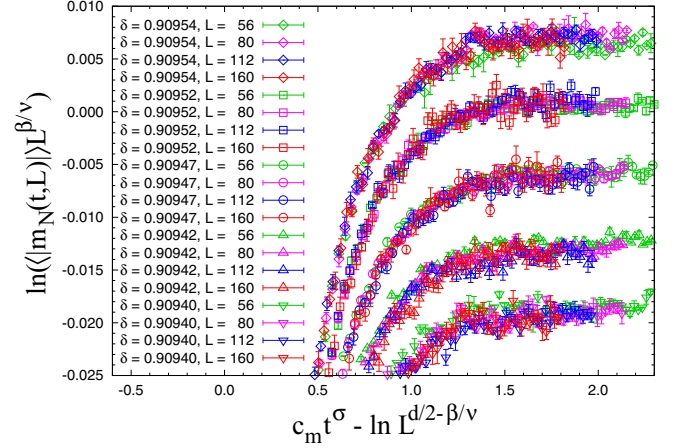

FIG. 5. Nonequilibrium-to-equilibrium scaling plot of the absolute value of the Néel order in the vicinity of equilibrium at $\delta = 0.909\,54$ (diamonds with $\beta/\nu = 0.517$), 0.909 52 (squares with $\beta/\nu = 0.516$), 0.909 47 (circles with $\beta/\nu = 0.514$), 0.909 42 (triangles with $\beta/\nu = 0.512$), and 0.909 40 (inverse triangles with $\beta/\nu = 0.511$) for $L = \beta = 56$ (green symbols), 80 (pink symbols), 112 (blue symbols), and 160 (red symbols) using $\sigma = 0.502$ and $c_m = 0.423$ used in Fig. 3 at $\delta = 0.909\,47$, for all the data in this figure. The data except for $\delta = 0.909\,47$ are shifted upward or downward for clear visualization.

out of scaling. Here the data for $L = 80$ and 112 are tuned to be scaled on a single curve. Then, deviations of the data for $L = 56$ and 160 are in opposite directions, and all the data cannot be scaled on a single curve anymore. We assign the error bars of our final estimates by including the widest variance of all the results as

$$\delta_c = 0.909\,47(6), \tag{10}$$

$$\beta/\nu = 0.514(3), \ \sigma = 0.501(9), \ c_m = 0.427(18). \tag{11}$$

These estimates are consistent with the previous ones for the same model based on large-scale equilibrium QMC simulations [22], $\delta_c = 0.909\,47(3)$ and $\beta/\nu = 0.513(9)$, and with ours for the 3D classical Heisenberg model based on the cluster NER [18], $\beta/\nu = 0.515(5)$ and $\sigma \approx 1/2$. Although the evaluation of δ_c based on the deviation of data in Fig. 5 is rather subtle, that of β/ν based on the scaling formula (8) is promising, where the wide scaling region results in high precision in comparison with a simple power-law fitting of equilibrium data [22], though accuracy of the estimation is still not comparable to that of a detailed study on critical phenomena in the 3D classical Heisenberg model, $\beta/\nu = 0.5189(12)$ [25], which is consistent with our estimate within 2σ.

B. Staggered susceptibility

Next, we analyze the staggered susceptibility using the estimates of δ_c and σ in Eqs. (10) and (11) and evaluate the critical exponent γ/ν. In Fig. 6, the data at $\delta = 0.909\,52$ (squares), 0.909 47 (circles), and 0.909 42 (triangles) for $L = 56$ (green symbols), 80 (pink symbols), 112 (blue symbols), and 160 (red symbols) are plotted using $\sigma = 0.501$ [the most
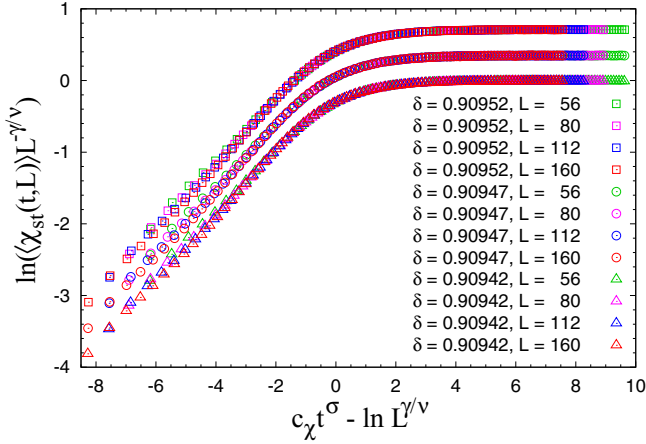
FIG. 6. Nonequilibrium-to-equilibrium scaling plot of the staggered susceptibility at $\delta = 0.909\,52$ (squares), $0.909\,47$ (circles), and $0.909\,42$ (triangles) for $L = \beta = 56$ (green symbols), 80 (pink symbols), 112 (blue symbols), and 160 (red symbols) using $\sigma = 0.501$ in Eq. (10), with $\gamma/\nu = 1.9703(8)$ and $c_\chi = 1.7480(24)$, $\gamma/\nu = 1.9730(8)$ and $c_\chi = 1.7484(26)$, $\gamma/\nu = 1.9752(8)$ and $c_\chi = 1.7488(26)$, respectively. Error bars are much smaller than symbols in this scale. The data except for $\delta = 0.909\,47$ are shifted upward or downward for clear visualization.

probable value in Eq. (11)]. The data at $\delta = 0.909\,47$ are scaled with $\gamma/\nu = 1.9730(8)$ and $c_\chi = 1.7484(26)$. Similarly using $\sigma = 0.492$ and 0.510, we have $\gamma/\nu = 1.9733(8)$, $c_\chi = 1.8283(29)$ and $\gamma/\nu = 1.9727(8)$, $c_\chi = 1.6727(24)$, respectively. To include all these estimates, we have $\gamma/\nu = 1.9730(11)$ and $c_\chi = 1.751(81)$ using $\sigma = 0.501(9)$. When the above procedure is repeated at $\delta = 0.952$ and 0.942 using $\sigma = 0.501(9)$, we have $\gamma/\nu = 1.9703(11)$, $c_\chi = 1.751(81)$ and $\gamma/\nu = 1.9752(12)$, $c_\chi = 1.751(81)$, respectively. To include all these scaling results, we finally have

$$\gamma/\nu = 1.973(4), \quad c_\chi = 1.75(8). \tag{12}$$

This estimate is consistent with ours in the 3D classical Heisenberg model based on the cluster NER [18], $\gamma/\nu = 1.972(7)$, and it satisfies $2\beta/\nu + \gamma/\nu = 3.001(6)$, which is consistent with the hyperscaling relation, $2\beta/\nu + \gamma/\nu = d + 1$, with the spatial dimension $d = 2$ plus the imaginary-time dimension. Consistency with the detailed estimate in the 3D classical Heisenberg model, $\gamma/\nu = 1.9622(43)$ [25], is still within 2σ.

IV. SUMMARY AND DISCUSSION

In the present article, we generalized the cluster nonequilibrium-relaxation (NER) scheme to quantum phase transitions. Since modern quantum Monte Carlo algorithms such as the loop algorithm are based on cluster updates, the present scheme is indispensable for the NER analysis of quantum systems. As an example, we considered the Néel-dimer quantum phase transition in the two-dimensional $S = 1/2$ columnar-dimerized antiferromagnetic Heisenberg model on a square lattice. This model is the simplest isotropic quantum spin system to exhibit a quantum phase transition

with respect to the strength of dimerization δ, and it belongs to the universality class of the 3D classical Heisenberg model.

In the present study, numerical calculations were based on the continuous-time loop algorithm with the Ising basis and started from one of the typical classical states consisting of the isolated dimer state. Although we have numerically and theoretically clarified that physical quantities at the critical point show stretched-exponential relaxation behavior in the early-time relaxation in cluster algorithms in classical spin systems, this behavior is not trivial in the present case, because one-dimensional loop clusters are geometrically different from the bulky ones in the Swendsen-Wang and Wolff algorithms. We confirmed this behavior and estimated the critical point δ_c, critical exponents β/ν and γ/ν, and relaxation exponent σ from the nonequilibrium-to-equilibrium scaling plot of the absolute value of the Néel order and staggered susceptibility as in our previous study on the 3D classical Heisenberg model. The present estimates $\delta_c = 0.909\,47(6)$, $\beta/\nu = 0.514(3)$, $\gamma/\nu = 1.973(4)$, and $\sigma = 0.501(9)$ are comparable to previous studies. Consistency with the 3D classical Heisenberg model holds not only for β/ν and γ/ν but also for σ. These results reveal that the cluster NER scheme can be generalized to quantum phase transitions on the basis of the continuous-time loop algorithm.

Finally, we discuss essential merits of the present scheme in quantum phase transitions. Since the simplest model was treated in the present article, the relaxation process was very fast, and advantages in comparison with equilibrium simulations were not so clear. Nevertheless, when the relaxation process is much slower, for example in a system on the edge of the weak first-order and second-order phase transitions, the advantage becomes more evident. The nonequilibrium-to-equilibrium scaling holds with the relaxation process including the initial stretched-exponential region and part of the transient region toward equilibrium. The former is rather short even for slow relaxation and the latter becomes long for that case, and we can terminate simulations much earlier than the conventional equilibrium ones.

The other essential merit arises for random systems. As shown in the present article, large numbers of random-number sequences should be averaged for accurate data in the NER analysis, and such averaging can be replaced by sample averaging in random systems. This fact indicates that numerical efforts in random systems may not be so different from pure systems. In the equilibrium Monte Carlo simulations, on the other hand, long-time measurement in a single sample results in a reduction of sample averaging. As measurement for each sample is reduced, the ratio of discarded data in simulations increases and efficiency of simulations decreases. Such a dilemma does not exist in the NER analysis. Studies along these directions are now in progress.

[1] H. F. Trotter, Proc. Am. Math. Soc. **10**, 545 (1959).

[2] M. Suzuki, Prog. Theor. Phys. **56**, 1454 (1976).

[3] B. B. Beard and U.-J. Wiese, Phys. Rev. Lett. **77**, 5130 (1996).

[4] H. G. Evertz, G. Lana, and M. Marcu, Phys. Rev. Lett. **70**, 875 (1993).

[5] N. V. Prokov'ev, B. V. Svistunov, and I. S. Tupitsyn, Sov. Phys. JETP **87**, 310 (1998).

[6] O. F. Syljuåsen and A. W. Sandvik, Phys. Rev. E **66**, 046701 (2002).

[7] As a review on the NER method, Y. Ozeki and N. Ito, J. Phys. A **40**, R149 (2007).

[8] R. H. Swendsen and J.-S. Wang, Phys. Rev. Lett. **58**, 86 (1987).

[9] U. Wolff, Phys. Rev. Lett. **62**, 361 (1989); Nucl. Phys. B **322**, 759 (1989).

[10] B. A. Berg and T. Neuhaus, Phys. Rev. Lett. **68**, 9 (1992).

[11] K. Hukushima and Y. Nemoto, J. Phys. Soc. Jpn. **65**, 1604 (1996).

[12] F. Wang and D. P. Landau, Phys. Rev. Lett. **86**, 2050 (2001).

[13] Completely disordered states are chosen as initial states in the present study, and we also take different initial configurations in individual MC runs.

[14] Y. Nonomura, J. Phys. Soc. Jpn. **67**, 5 (1998); J. Phys. A **31**, 7939 (1998).

[15] T. Nakamura and Y. Ito, J. Phys. Soc. Jpn. **72**, 2405 (2003).

[16] Y. Nonomura, J. Phys. Soc. Jpn. **83**, 113001 (2014).

[17] Y. Nonomura and Y. Tomita, Phys. Rev. E **92**, 062121 (2015).

[18] Y. Nonomura and Y. Tomita, Phys. Rev. E **93**, 012101 (2016).

[19] Y. Tomita and Y. Nonomura, Phys. Rev. E **98**, 052110 (2018).

[20] M. Matsumoto, C. Yasuda, S. Todo, and H. Takayama, Phys. Rev. B **65**, 014407 (2001).

[21] S. Wenzel and W. Janke, Phys. Rev. B **79**, 014410 (2009).

[22] S. Yasuda and S. Todo, Phys. Rev. E **88**, 061301(R) (2013).

[23] As a review on the loop algorithm, N. Kawashima and K. Harada, J. Phys. Soc. Jpn. **73**, 1379 (2004).

[24] During the nonequilibrium-relaxation process from the isolated dimer state, the (2, 1)-Binder ratio $B_{2,1}(t, L) \equiv \langle m_N^2(t, L)\rangle / \langle |m_N(t, L)|\rangle^2$ shows a nontrivial peak after several MCS, even though it is expected to decrease monotonically from the Gaussian value $\pi/2$.

[25] M. Campostrini, M. Hasenbusch, A. Pelissetto, P. Rossi, and E. Vicari, Phys. Rev. B **65**, 144520 (2002).

[26] M. Matsumoto and T. Nishimura, ACM TOMACS **8**, 3 (1998), further information is available from the Mersenne Twister Home Page, http://www.math.sci.hiroshima-u.ac.jp/~m-mat/MT/emt.html.